Effect of aging on the removal of asphaltene deposits with aromatic solvent

Sophie Margaret Campen[1], Saul J. Moorhouse[2] and Janet S. S. Wong[1]*

[1]Department of Mechanical Engineering, Imperial College London, UK SW7 2AZ

[2]BP Exploration Operating Company Limited, Chertsey Road, Sunbury-on-Thames, Middlesex, UK TW16 7LN

*Corresponding author. Telephone: +44 (0)20 7594 8991. E-mail: j.wong@imperial.ac.uk

Abstract

Surface-deposition of destabilized colloidal particles of asphaltenes poses a serious and costly problem during petroleum production. Remediation of asphaltene-fouled well-bore and surface facilities is often undertaken by flowing aromatic solvent to remove deposited films. However, little is known about the properties of deposited asphaltene films during their removal by solvent-rinsing. Here, we carry out quartz crystal microbalance with dissipation monitoring (QCM-D) experiments to investigate surface-deposition of destabilized colloidal particles of asphaltenes and their subsequent removal by solvent-rinsing. It is shown that the properties of deposited films during solvent removal depend on the history of the deposit. Newly formed deposit films are removed immediately without significant change in their mechanical properties during removal. However, deposits that remain on the surface for an extended time in a poor solvent (a low-asphaltene solubility solvent), "aged deposits", are more difficult to remove and exhibit increased dissipation during the removal period, indicating that they swell and are softer. Liquid-cell atomic force microscopy (AFM) confirms that aged deposits swell when the quality of the solvent is subsequently improved by exchanging for a high-asphaltene solubility solvent. Deposit swelling is accompanied by a change in film morphology, from particulate to continuous. Stubborn deposits of aged asphaltene films, which remain after solvent-rinsing, may be partly removed by flowing dissolved asphaltenes in good solvent. Hence, reinjection of asphaltenes during remediation can aid deposit removal.

Introduction

In many industries, the formation of organic films is unwanted and constitutes 'fouling'. One such industry is petroleum production, where organic deposits of asphaltenes reduce the efficiency of operations [1]. Thick deposits of asphaltenes may be removed by rinsing with solvent or by mechanical scraping. Much research has been carried out to understand asphaltenes aggregation [2,3,4] and deposition behaviours

[5,6,7,8,9,10,11]. However, little is known about what happens to deposits during their removal by solvent-rinsing.

Asphaltenes are the densest, most polar fraction of crude oil and consist of an array of different molecular structures that contain polycyclic aromatic hydrocarbons [12]. Asphaltenes are a solubility class defined as soluble in toluene and insoluble in n-heptane. Although described as toluene-soluble, asphaltenes may actually exist as a colloidal dispersion of nanoaggregates, depending on their concentration [13]. When asphaltenes are destabilized by adding n-heptane, they form larger particles, clusters and large aggregates, which may precipitate or deposit onto surfaces [14]. Destabilized nanoaggregates initially undergo reaction-limited aggregation, however at longer destabilization times there is cross-over to diffusion-limited aggregation [2]. Aggregation rate depends on both precipitant concentration and the type of crude oil [4]. Destabilized insoluble asphaltene aggregates exhibit increasing fractal dimension with aggregate size, and flocculated asphaltenes may have discoid structure [3]. Current research finds that surface-deposition is largely due to adhesion of destabilized submicrometer aggregates rather than adhesion or sedimentation of large floccules; and aged dispersions do not deposit [15]. Deposition rate increases linearly with increasing concentration of destabilized asphaltenes and is diffusion limited for depositing nanoparticles [7]. The flow regime can also have a significant impact and deposits may preferentially grow in low shear zones [10].

The heptane-toluene ratio used to destabilize asphaltenes has several important effects: (1) on the rate of asphaltene aggregation – how the particle size distribution evolves with time, (2) on the proportion of asphaltenes that will eventually precipitate at equilibrium and (3) on the respective chemistries of the soluble and insoluble subfractions, see Fig 1 [16,17]. Thus, when we change the heptane vol% used to destabilize asphaltenes, we may alter the properties of the deposited film – both its morphology and its chemistry [18,19].

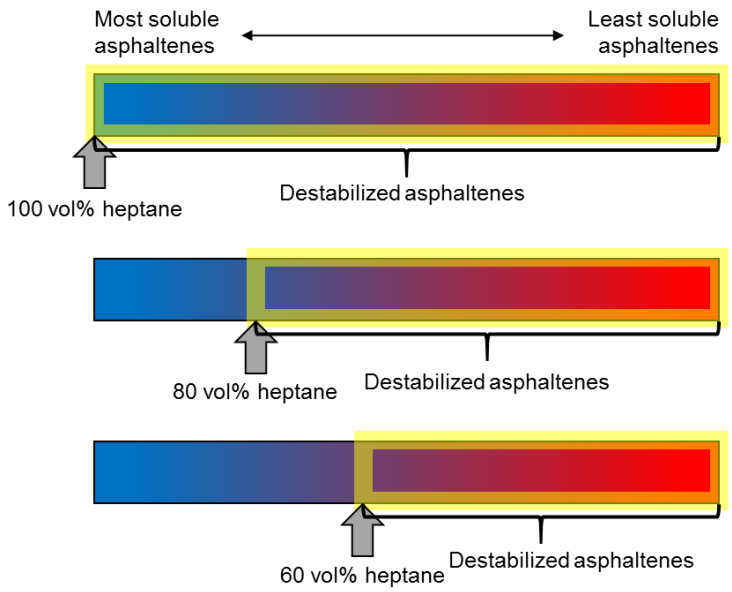

Fig 1. Diagram illustrating impact of heptane volume fraction on relative solubility of destabilized asphaltenes

Previously, we have seen a mismatch between laboratory studies and observations of asphaltene deposition in the field. In laboratory studies, solvent-rinsing of asphaltene deposits resulted in almost instantaneous removal [18]. However, in the field, deposits are not so easily removed. There are many differences between laboratory conditions and operating conditions. The first is the time-scale. Deposition experiments in the laboratory are relatively short (typically lasting less than an hour), while in reality deposits may build up over days, weeks and years. Secondly, typical laboratory experiments use asphaltenes extracted from depressurised crude oil samples, therefore contributions from other chemistries within the crude oil (including inorganic salts and some low solubility asphaltene fractions) will be absent or diminished [20]. Thirdly, there are differences in environmental conditions (temperature, pressure) and liquid flow rate. Here, we focus on understanding the impact of time-scale.

Quartz crystal microbalance with dissipation monitoring (QCM-D) has been used to investigate deposition of asphaltenes from toluene [21,22,23] and heptane-toluene [24]. Since dissipation is a measure of the quartz crystal's dampening, it is sensitive to the nature of the deposited film. Hence, in addition to providing information on the deposited mass, QCM-D also gives information on the material properties of deposits. It has been used to monitor adsorbed vesicle to lipid bilayer transitions [25], pH-sensitive swelling of polymer brushes [26], thermally-induced swelling and collapse of polymer brushes [27], protein cross-linking [28] and cooling-induced crystallisation of sulfamerazine [29].

In this paper, we use QCM-D to investigate the material properties of colloidal films of asphaltenes during their deposition and subsequent removal by solvent-rinsing. In-line mixing of asphaltenes in toluene with

heptane-toluene upstream of the in situ QCM is used to generate destabilized colloidal dispersions which give rise to surface deposition inside the QCM. We study the impact of aging deposits in poor (high-heptane) solvent on both their ease of removal and their material properties. To achieve this, we carry out 3-stage experiments which involve flowing different liquids over a surface: (i) asphaltenes in heptane-toluene, (ii) heptane-toluene and (iii) pure toluene or asphaltenes in toluene. In stage (i) a multilayer deposit is formed. In stage (ii) the deposited film is aged, without significant change in mass. In stage (iii) the deposit is removed by solvent-rinsing. By varying the duration of stage (ii), or omitting it completely, we are able to compare the removal of aged deposits with that of fresh (unaged) deposits. Liquid-cell AFM is used to probe the morphology of asphaltene deposits formed in-situ and the impact of changing heptane-toluene solvent-environment.

Experimental Section

Materials and preparation techniques

A crude oil sample was provided by BP. The n-heptane insoluble fraction of crude oil (asphaltenes) was extracted by adding an excess of n-heptane to crude oil (40:1 mass ratio), agitating in an ultrasonic bath for 1 h, aging in a dark cupboard for 2 d, collecting the precipitate by vacuum filtration (0.45 µm pore PTFE filter, Merck Millipore), rinsing with excess of n-heptane until the filtrate was colourless, and then drying in an oven at 70°C for 1 h. Asphaltenes were then dispersed in toluene to give a 10 gL^{-1} stock solution, homogeneity was ensured by ultrasonicating prior to use. This stock solution was stored in a dark cupboard and aliquots diluted as required. n-heptane (≥99%, CHROMASOLV) and toluene (99.9%, CHROMASOLV) used as precipitant-solvent were acquired from Sigma-Aldrich and used without further purification.

Gold-coated QCM sensors (Biolin Scientific) were used as model metallic surfaces for deposition studies (note that oil pipes are typically made of steel). During QCM experiments, sensors were held in temperature-controlled titanium flow cell with Kalrez O-ring and gasket. The dismantled flow cell and QCM sensors were cleaned by rinsing with toluene, acetone and air drying. The parts were ultrasonicated for 30 min in Hellmanex III cleaning solution (2 vol% in DI H_2O, Millipore Milli-Q resistivity >18.2 MΩ cm) before rinsing thoroughly under running DI water. The parts were then rinsed with acetone and dried under a stream of N_2 gas. The QCM sensor was cleaned under oxygen plasma (Diener Atto low pressure plasma cleaner) for 2 min which yields the gold surface hydrophilic. Hellmanex III and acetone (≥99.8%, CHROMASOLV) were acquired from Sigma-Aldrich. Highly-polished steel discs (AISI 52100), used as substrates for AFM deposition studies, were acquired from PCS Instruments (Acton, UK) and cleaned by ultrasonicating in toluene for 10 min before use.

QCM-D apparatus

QCM utilizes the piezoelectric effect of quartz to obtain quantitative information about changes in environment. An AC voltage is applied to a thinly-cut quartz crystal sensor to make it oscillate at its fundamental frequency (f_0). Here, we use a sensor with f_0 = 5 MHz. The sensor is also oscillated at odd overtones (n) of f_0 having frequencies f_n = 15 (n=3), 25 (n=5), 35 (n=7), 45 (n=9), 55 (n=11) and 65 (n=13) MHz. In QCM-D (Biolin Scientific), the driving voltage is intermittently switched off and the oscillation of the crystal observed to decay exponentially. The rate of decay is a measure of the crystal's dissipation (D):

$$\mathrm{D} = \frac{E_{lost}}{2\pi E_{stored}} \qquad \text{Equation 1}$$

where E_{lost} is the energy lost in one complete oscillation and E_{stored} is the energy stored in the oscillating crystal.

Frequency and dissipation are sensitive to the environment of the quartz crystal and shifts in these values are observed (1) when changing from air to liquid, (2) when exchanging between two liquids of different viscosity and/or density, and (3) when mass is adsorbed or deposited onto the sensor surface. In most adsorption studies, shifts in frequency and dissipation are measured relative to the same solvent in which the adsorbing / depositing species are dissolved / dispersed.

In the case of thin, rigid adsorbed films, the Sauerbrey mass may be used [30]. In reality, adsorbed films are often thick and 'lossy' or dissipative. In some cases, an appropriate viscoelastic model (e.g. Voigt or Maxwell) may be used to model the adsorbed film as a homogenous layer. However, these models may be unsuitable for films that are inhomogeneous or particulate [31]. In these cases, the adsorbed mass cannot be simply obtained and the raw frequency and dissipation data may be interpreted directly. Previously, we showed that the Voigt viscoelastic model could reasonably approximate the deposited mass of asphaltene films [18]. We use Q-Tools software to model data from all available overtones (omitting the fundamental) to obtain deposit mass (and thickness). The density of the asphaltene film is assumed to be 1.2 gcm^{-3} based on literature [32,33].

QCM-D adsorption and deposition studies

We have carried out numerous deposition-aging-rinsing studies in the QCM-D. We use a two reservoir-two pump system to generate destabilized dispersions of asphaltenes in heptane-toluene, as described previously [18]. Asphaltenes (1 gL^{-1}) solution in toluene is held in the first reservoir and is pumped at a

flow rate of 2 μLs^{-1} by an Ismatec Reglo 12-roller pump with Viton Tubing. Heptane-toluene is held in the second reservoir and is pumped at a flow rate of 18 μLs^{-1} by a Global FIA milliGAT HF pump. These liquids meet at a mixing T-junction (static PEEK Tee with internal swept volume of 17.3 µL together with inlet check valves to prevent liquid backflow, from Kinesis Ltd.) and then flow through a 1/32" internal diameter PTFE tube of 60 cm length towards the QCM flow cell. After the T-junction, asphaltenes (0.1 gL^{-1}) in heptane-toluene flows at a rate of 20 μLs^{-1}. This method ensures that destabilization time, the time taken for the mixture to travel from the T-junction to the QCM sensor, is fixed at 20 s. This results in a constant particle size distribution of asphaltene above the QCM sensor surface during the deposition among tests. Liquid-liquid mixing and asphaltene destabilization occurs inside the T-junction, the PTFE tubing and also the internal flow path inside the QCM flow cell. Flow is laminar, Re = 49 (in toluene) to 61 (in 90 vol% heptane) inside the PTFE tube. The serpentine flow path inside the QCM flow cell consists of a series of 10 U-bends, which ensures mixing is complete before the liquid eventually reaches the sensor surface. This internal flow path also permits temperature equilibration to 20°C, which is used for all experiments. Before flowing asphaltene, baselines are acquired in solvent only. A typical experimental procedure involves the following steps: (1) obtain baseline in toluene, (2) obtain baseline in heptane-toluene, (3) obtain baseline in toluene, (4) asphaltenes adsorption in toluene (monolayer adsorption), (5) asphaltenes deposition in heptane-toluene (multilayer deposition), (6) expose deposits to heptane-toluene (asphaltene deposit 'aging') and (7) expose deposits to toluene (asphaltene deposit removal by solvent-rinsing).

Liquid-cell AFM adsorption and deposition studies

Deposition-aging-rinsing experiments were made inside the liquid-cell AFM using the same two reservoir-two pump system as for QCM-D. A Bruker Multimode AFM with Nanoscope V controller was used with a MTFML-V2 liquid-cell with Viton O-ring. DNP-S triangular cantilevers with 0.12 Nm^{-1} nominal spring constant and 23 kHz nominal resonance frequency (Bruker AFM Probes) were used to acquire images in contact and tapping modes. During asphaltene deposition, the tip was retracted from the surface to avoid interference of the scanning tip with the deposition process. Thick asphaltenes deposits on the AFM tip surface and on the steel substrate were removed by repeatedly scanning a small $10 \times 10\ \mu m^2$ area under increased load (50 nN) in contact mode. The AFM tip was also retracted during changing heptane vol% and the angle of the mirror (which aligns the reflected laser beam from the AFM cantilever onto the photodetector) adjusted to compensate for the changing refractive index of the liquid.

Results and Discussion

QCM-D liquid-loading effects during changing heptane-toluene ratio

Before asphaltenes deposition, baselines are obtained in toluene and heptane-toluene. A typical baseline measurement as we go from pure toluene to 60 vol% heptane and back to pure toluene is shown in Fig 2 (a). Shifts in frequency and dissipation are caused by changing viscosity and density, Fig 2 (b), which alter the QCM-D sensor response, Fig 2 (c). This is called the liquid-loading effect. Note that the addition of asphaltene into toluene may also result in this effect. Since the concentration of asphaltenes used in experiments is very low (0.1 gL^{-1}), the liquid-loading effect caused by the presence of asphaltenes is negligible, see Table S2. Hence, the main liquid-loading effect that we must account for is that of the changing heptane-toluene ratio, see Table S1.

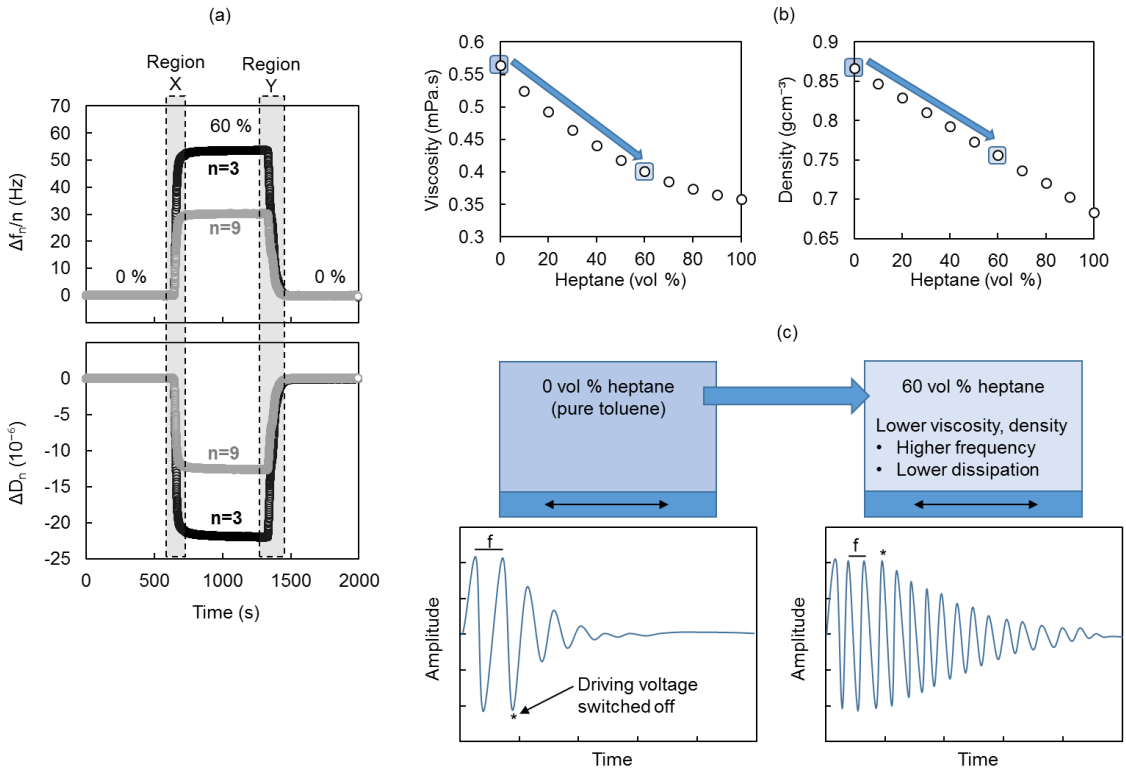

Fig 2. (a) Frequency and dissipation shifts upon changing from pure toluene to 60 vol% heptane then back to toluene, illustrating the Liquid-loading effects. The percentage of heptane is stated in the top graph. Regions X and Y denote transitional periods where properties of the liquid are changing, (b) viscosities and densities of heptane-toluene solutions from Stabinger viscometer, and (c) graphical representation of changing QCM-D sensor response in different solutions.

We can create a plot of dissipation vs. frequency for this measurement, Fig 3 (a). A straight line is obtained and the data from different overtones overlaps. The frequency and dissipation shifts due to the changing properties of the bulk liquid (as we go from liquid 1 to liquid 2) are given by [34,35]:

$$\Delta f_n = -\sqrt{\frac{n}{\pi}}\frac{{f_0}^{\frac{3}{2}}}{\rho_q \nu_q}\left(\sqrt{\rho_2\eta_2} - \sqrt{\rho_1\eta_1}\right) \qquad \text{Equation 2}$$

$$\Delta D_n = \frac{1}{\sqrt{n\pi}}\frac{2{f_0}^{1/2}}{\rho_q \nu_q}\left(\sqrt{\rho_2\eta_2} - \sqrt{\rho_1\eta_1}\right) \qquad \text{Equation 3}$$

where ρ_q is the specific density of quartz, ν_q is the shear wave velocity in quartz, ρ_1 and η_l are the density and viscosity respectively of liquid 1, and ρ_2 and η_2 are the density and viscosity respectively of liquid 2.

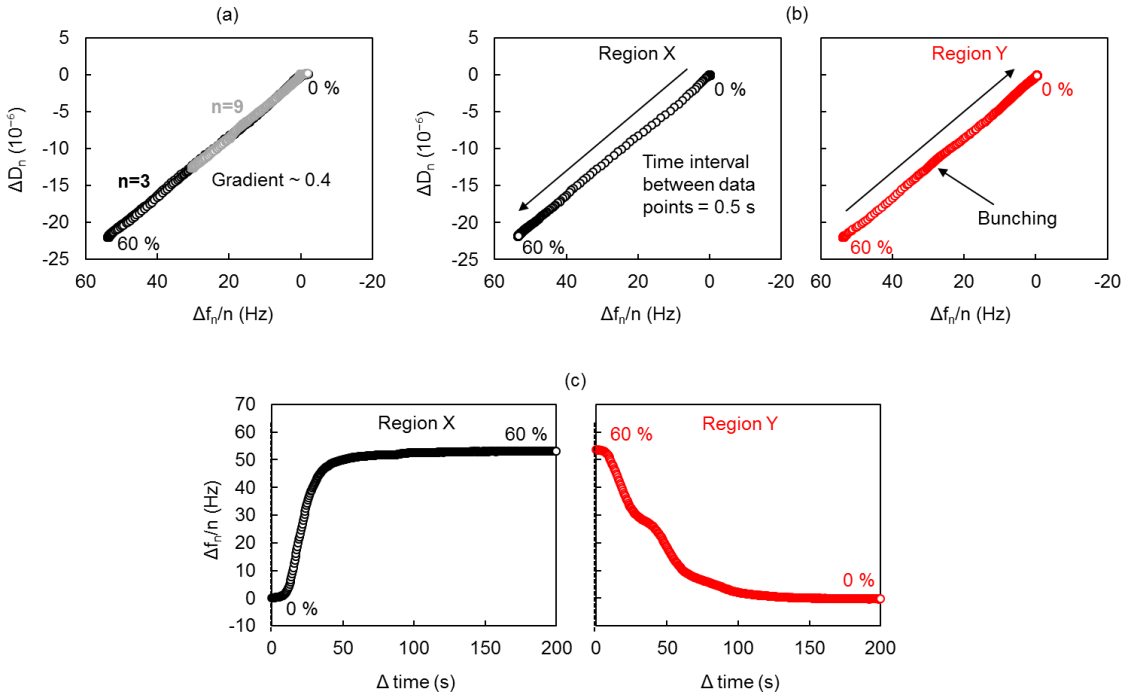

Fig 3. Liquid-exchange dynamics. (a) Frequency-dissipation plot for baseline measurements in pure toluene and 60 vol% heptane based on Fig 2 (a), (b) data point distribution for n=3 for regions X (black, increasing heptane vol%) and Y (red, decreasing heptane vol%) and (c) frequency shifts for regions X (black) and Y (red) from Fig 2(a) vs. relative time from the start of the transitions.

Note that the terms in brackets in Equations 2 and 3, which describe the changing properties of the liquid, are the same. By re-arranging and substituting, we obtain:

$$\Delta D_n = -\frac{\Delta f_n}{n}\left(\frac{2}{f_0}\right) \approx -\frac{\Delta f_n}{n} \times 0.4 \times 10^{-6} \qquad \text{Equation 4}$$

which effectively describes the data shown in Fig 3 (a), remember, f_0 ~ 5 MHz. It is observed that the heptane concentration sensed by the QCM sensor changes gradually from 0 to 60 vol% heptane (Region X) and from 60 to 0 vol% heptane (Region Y). Data from regions X and Y are separately plotted in Fig 3 (b). It shows clearly that the data points are not evenly spaced. The transitional period (where the properties of the bulk liquid are changing) lasts ~ 30 seconds and is smooth when going from 0 to 60 vol% heptane (Fig 3 (c)). While the reverse process, going from 60 to 0 vol%, is much longer (~ 100 seconds) and is less smooth. This is an artefact of the milliGAT pump which is used to pump heptane-toluene. The behaviour is reproducible even when exchanging to 80 vol% heptane, see Fig S1.

The time taken to exchange between two liquids depends on the heptane-toluene concentration gradient reaching the QCM. For our experiment, this can be influenced by a combination of factors including the flow velocity profile (flow is pressure-driven), the residency time from the T-junction to the QCM sensor, the nature of the flow path, the relative diffusivities of heptane and toluene, and the type of pump used to flow the liquids. There is also a response time of approx. 5 seconds as we switch from one solvent to another in our setup. All these may contribute to the observed transition period in Fig 3 (c). Hence, routinely subtracting the liquid-loading effects for the liquid-exchange period is non-trivial. It would require high confidence in the reproducibility of the temporal variation of heptane concentration during the transitional period and the determination of the exact time at which liquid-exchange begins. Since the relative changes in frequency and dissipation at the beginning of liquid-exchange are small, pinpointing the exact start-point is not straightforward. An asymptotic solution for the liquid-exchange start-point may not be obtained if there are simultaneous changes in adsorbed mass. In QCM-D adsorption studies, one may choose only to analyse data obtained when the properties of the bulk liquid were constant with time, i.e. data in transitional periods are omitted. This is adequate for most studies. However, in some cases, particularly where the rate of change in adsorbed mass is very fast, changing adsorbed film properties may be completely masked by the changing liquid properties, as shown next.

Removal of unaged deposits by solvent-rinsing

In initial studies, deposited asphaltene films were immediately rinsed with asphaltene solution in toluene, i.e. they were not aged. An example deposition-rinsing experiment is shown in Fig 4 (a). Frequency and dissipation shifts are plotted relative to those of an asphaltene monolayer in 0.1 gL^{-1} asphaltene solution in toluene (0 vol% heptane). When the heptane fraction is increased to 80 vol% (arrow with '80%' label), the frequency initially increases (due to the liquid-loading effect) and then decreases (due to multilayer mass deposition). After the deposition, we return to 0 vol% heptane (arrow with '0%' label), and Δf and

ΔD return to the baseline value for a single asphaltene monolayer almost instantaneously. This suggests that deposit removal during solvent-rinsing occurs readily. In fact, most mass is removed in ~ 40 s, which is shorter than the time taken to completely transition from heptane-toluene to toluene, which takes ~ 100 s.

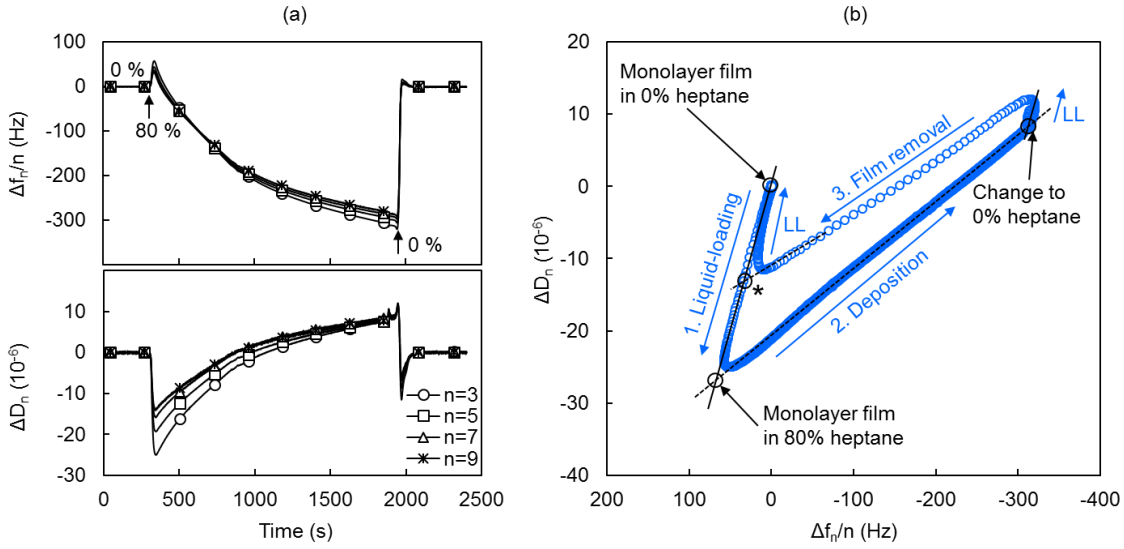

Fig 4. Deposition and removal of colloidal film. (a) Frequency and dissipation shifts showing 0.1 gL^{-1} asphaltenes deposition from 80 vol% heptane (arrow with '80 %' label) and subsequent removal in 0 vol% heptane (arrow with '0 %' label), (b) frequency-dissipation plot for n=3 of the whole experiment. Shifts are relative to a pre-adsorbed asphaltene monolayer film in 0.1 gL^{-1} asphaltenes in 0 vol% heptane. Additional regions of liquid-loading (LL) upon returning to 0 vol% heptane are indicated.

To obtain information on the nature of the asphaltene deposit during its removal, we look to the frequency-dissipation plot, Fig 4 (b). Three distinct regions, corresponding to (1) liquid-loading, (2) deposition and (3) film removal, are observed. A closed loop is obtained, confirming that the multilayer deposit is completely removed, leaving only the monolayer film. During regions of mass-loading (deposition) and mass-unloading (film removal), the gradient of the frequency-dissipation plot reveals the relative change in dissipation per change in unit mass (frequency) of the film [36]. A film that is rigid will dissipate very little energy and thus the slope of the frequency-dissipation plot will be very low. A film that is not rigid (e.g. soft viscoelastic or weakly bound) will have higher relative dissipation and thus a steeper slope will be observed [37,38]. Since time is eliminated as a parameter, the properties of films that formed or were removed at different rates can be compared. In Fig 4 (b) the gradients of the lines during deposition and film removal are similar, suggesting that the mechanical properties of the film during its removal are similar to those during its deposition. Note that slight difference in gradient between the

deposition and removal regions is expected, given the simultaneously changing bulk liquid properties (liquid-loading effect). Upon changing from 80 to 0 vol% heptane, film removal occurs between regions dominated by liquid-loading effects where changing heptane vol% are accompanied with minimal change in mass (LL in Fig 4 b). This shows that the multilayer deposit is mostly removed at higher heptane vol%.

Asphaltene depositions were made at different heptane vol%, Fig 5. In all cases, the multilayer deposited films are readily removed by solvent-rinsing and the initial pre-adsorbed monolayer film is recovered. We can approximate the point at which most of the deposited mass is removed (* in Fig 5) and equate this to a heptane vol% using the viscosity and density data obtained with the Stabinger viscometer (Fig 2 b) together with equations 2 and 3. The actual heptane vol% at which most deposited mass is removed is lower for deposits formed at lower heptane vol %, see Table 1. This behaviour may be due to chemical differences among the deposits formed under different conditions. Remember that asphaltenes are a solubility class of crude oil, defined as being toluene-soluble and heptane-insoluble. Deposits formed at lower heptane vol % contain only the least soluble asphaltene molecules, see Fig 1, and therefore may be more difficult to remove, requiring a greater concentration of toluene in the solvent.

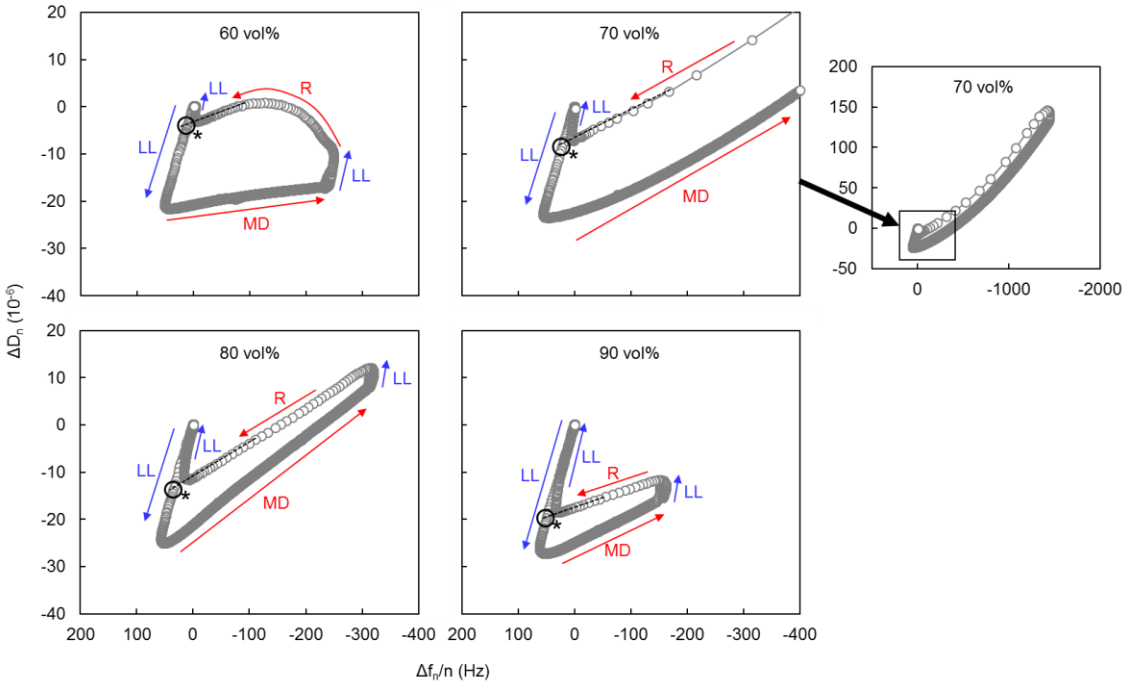

Fig 5. Effect of deposition conditions on removal of asphaltenes colloidal film. Frequency-dissipation plots for n=3 showing asphaltenes deposition from 60, 70, 80 and 90 vol% heptane, followed by removal in 0 vol% heptane. Regions of liquid-loading (LL), mass deposition (MD) and film removal (R) are marked. A deposition time of c. 30 min was used for each experiment. * indicates point used to determine heptane vol% at which most deposited mass is removed. All shifts are relative to a pre-adsorbed asphaltene monolayer film in 0.1 gL^{-1} asphaltenes in 0 vol% heptane.

Table 1. Effect of deposition conditions on ease of deposit removal. The heptane fraction at which the colloidal film is removed is calculated from the liquid-loading shifts at the point of removal (indicated as * in Fig 5).

Heptane fraction used for deposition (vol%)	Δf_3 (liquid-loading) at point of mass removal (Hz)	ΔD_3 (liquid-loading) at point of mass removal (10^{-6})	Calculated Viscosity · Density (kg m^{-3} · kg m s^{-1})	Heptane fraction at which deposit is removed (vol%)
60	11.0	-3.8	0.461	7
70	22.0	-8.2	0.424	16
80	36.2	-14.1	0.378	31
90	49.2	-19.4	0.338	41

Effect of aging on the removal of deposits by solvent-rinsing

The impact of aging on the removal of asphaltene deposits in 70 vol% heptane was investigated. After asphaltene deposition, aging in flowing heptane-toluene was carried out by switching the first reservoir from 1 gL^{-1} asphaltene in toluene to pure toluene. This meant that the heptane volume fraction was kept constant, i.e. the same as used for deposition, while preventing further asphaltene deposition. After a specified aging time, solvent rinsing was carried out by flowing 0 vol% heptane (pure toluene). There were no asphaltenes in the liquids used for aging and solvent-rinsing.

Deposit aging in poor (high heptane) solvent dramatically alters the mechanical properties of the deposited film during its removal, Fig 6. Aged films exhibit much higher dissipation during their removal, suggesting that they swell and are softer. The relative dissipation ($\Delta D_n/(-\Delta f_n/n)$) during solvent-rinsing, hence the amount of swelling, increases with both aging time and the deposited mass present before aging, see Fig S2 and Fig S3. A thick deposited film (214 nm thickness), aged for 4 h, exhibited very high dissipation during solvent-rinsing, Fig 6 (b). Although thicker films exhibit a larger amount of swelling, note that an *unaged* thick deposited film (246 nm thickness) was removed without swelling in 0 vol% heptane (Fig 5, 70 vol% heptane). Hence, aging in poor solvent is a pre-requisite for swelling.

Deposit aging also impacts how easily the deposited film is removed. Aged deposits are not removed as quickly as unaged deposits during solvent-rinsing. The time taken to remove the unaged deposit is 22 s. The deposit film that has been aged for 1 h, however, is removed in a much longer time of 198 s, see that the liquid-loading shift completes before all mass is removed, Fig 6 (a). The thick deposited film which had been aged for 4 h could not be completely removed, even after a total rinse-time in toluene of 70 min, Fig 6 (b). Note, the time taken to remove deposited films was determined directly from the frequency-

dissipation plots and incurs an error of +/- 5 s, see Fig S4. The impact of deposit aging upon its subsequent removal in toluene is reproducible, however further work is required to draw a quantitative relationship between aging time and amount of deposit swelling. The results show that deposit aging in poor solvent can contribute to the formation of strongly-bound deposits that cannot be easily removed with aromatic solvent. This agrees with a previous study which found that asphaltenes deposited in porous media micromodel could be completely removed if immediately rinsed with good solvent, but could not be removed if rinsed with a poor solvent followed by a good solvent [39].

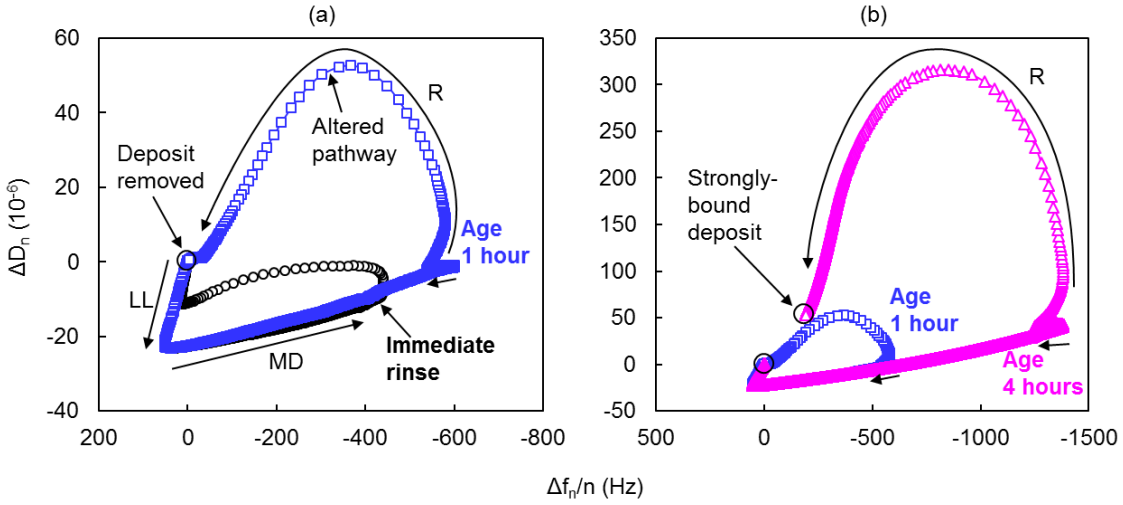

Fig 6. Impact of aging on removal of asphaltene colloidal film. Frequency-dissipation plots for n=3 showing asphaltenes deposition and aging in 70 vol% heptane, followed by removal in 0 vol% heptane. (a) Immediate removal (black circles) vs. 1 h aging (blue squares) and (b) 1 h (blue squares) vs. 4 h aging (pink triangles). Regions of liquid-loading (LL), mass deposition (MD) and film removal (R) are marked. Shifts are relative to a pre-adsorbed asphaltene monolayer film in 0.1 gL^{-1} asphaltenes in 0 vol% heptane.

Aging in poor solvent may allow more time for asphaltene-asphaltene binding which consolidates the film and makes it more difficult to remove. Additionally, if the more soluble (potentially resinous) asphaltenes are removed during aging in heptane-toluene, this may facilitate increased asphaltene-asphaltene interactions between the remaining, less soluble asphaltenes, resulting in a more-strongly bound film containing a higher proportion of lower solubility asphaltenes [40]. The removal of the more soluble asphaltenes from the deposited layer during aging may be enhanced by flowing heptane-toluene without dispersed asphaltenes in the liquid phase. Note that during aging there appears to be some mass loss (frequency becomes more positive), however the relative dissipation ($\Delta D_n/(-\Delta f_n/n)$) does not change appreciably, hence we perceive that significant morphological changes do not occur during the aging step. This supports the hypothesis that the more highly soluble asphaltenes are removed during aging.

Presently, we cannot determine whether the impact of aging is predominantly a time-effect or a solvent-environmental effect (i.e. that the deposit is impacted by removal of asphaltenes from the liquid phase). Indeed, it may be a time-limited solvent-environmental effect, in that the removal of the more soluble asphaltenes from the deposit occurs gradually during rinsing with heptane-toluene.

In this study, deposit aging is carried out under steady flow of heptane-toluene. This means that any desorbed asphaltenes will be carried out with the flow, which may drive further asphaltene desorption. In contrast, aging under a static condition would result in an increase in the concentration of desorbed asphaltenes in the liquid above the deposit. In this case a thermodynamic equilibrium may be reached between the dissolved and deposited asphaltenes. In such a scenario the impact of aging may be reduced relative to our dynamic flow conditions.

In a separate study, the quality of solvent flowing over an aged deposit during solvent-rinsing was gradually improved, Fig 7. Once again, the deposit is not removed in 0 vol% heptane (pure toluene). Flowing asphaltene solution in toluene (step labelled 'Asph' in Fig 7) removes a greater proportion of mass than toluene alone, thus asphaltene solution in toluene is a better solvent for the deposited asphaltenes than pure toluene (see increase in Δf, thick arrow in Fig 7 (c)). This supports the finding that dissolved asphaltenes play a key role in dispersing / solvating deposited asphaltenes. Dissolved asphaltenes in the liquid phase may therefore aid remediation.

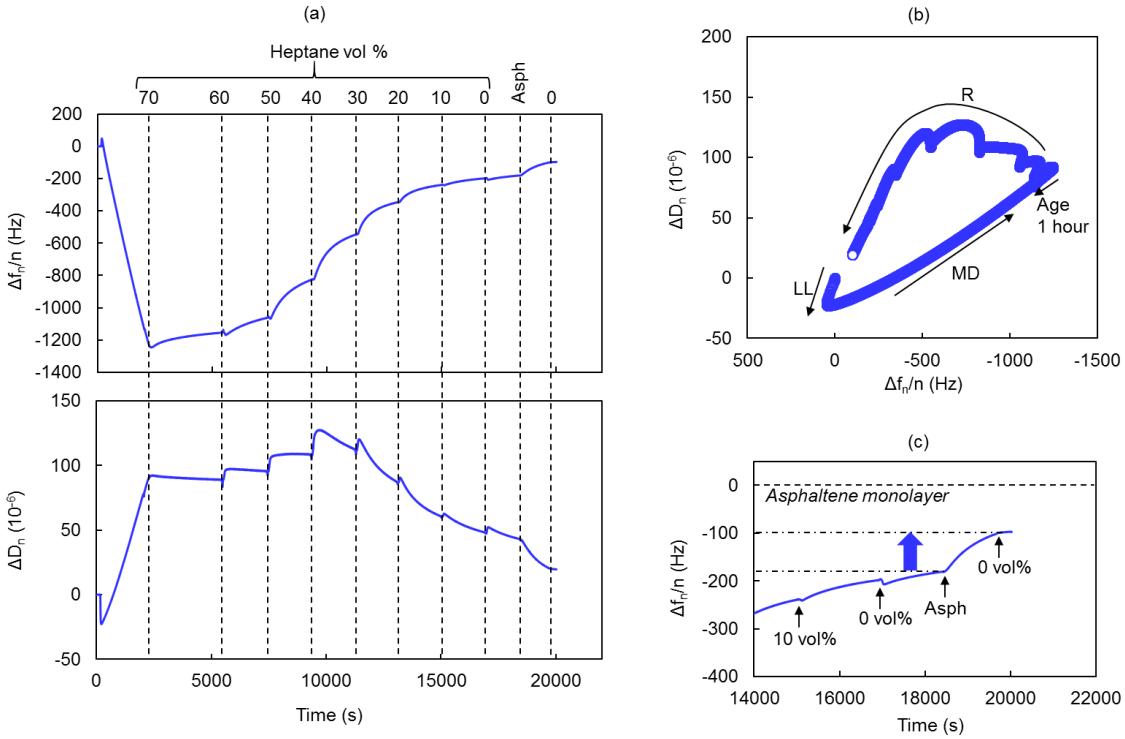

Fig 7. Removal of aged asphaltene deposits by gradual improvement in solvent quality. (a) Frequency and dissipation shifts showing 0.1 gL^{-1} asphaltenes deposition from 70 vol% heptane, followed by 1 h aging and removal in heptane-toluene, (b) frequency-dissipation plot for n=3, (c) final rinsing with 0.1 gL^{-1} asphaltenes in toluene (Asph) aids deposit removal. Shifts are measured relative to baseline in 0.1 gL^{-1} asphaltenes in 0 vol% heptane.

Reversibility of deposit swelling

The reversibility of deposit swelling was investigated. Aged deposits were rinsed with 40 vol% heptane, rather than pure toluene. This allowed deposit swelling, while preventing total mass removal. The result is that deposits are effectively trapped in the swollen state, i.e. near the top of the rinsing curve in the frequency-dissipation loop, as shown in Fig 8 (b). See also that ΔD has plateaued in Fig 8 (a). After some time, the heptane fraction was increased to 90 vol%. It is observed that there is a decrease in dissipation, suggesting that the film contracts and becomes more rigid, while the frequency remains largely unchanged, suggesting that the mass remains constant. The eventual film properties are nearer to those exhibited during deposition. This shows that film swelling is partly reversible and depends on the quality of the solvent in contact with the film.

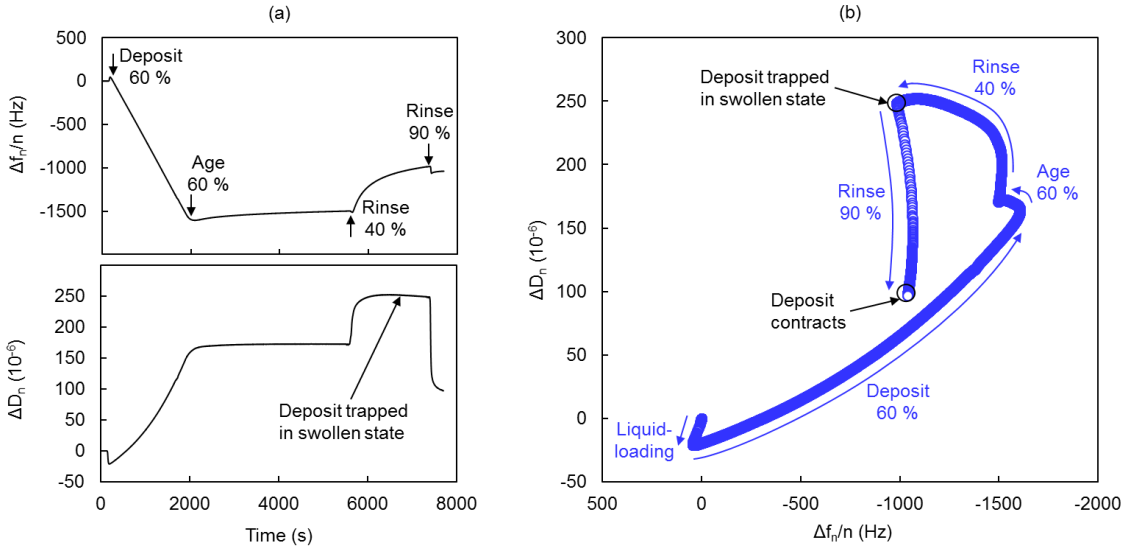

Fig 8. Reversibility of deposit swelling. (a) Frequency and dissipation shifts showing 0.1 gL^{-1} asphaltenes deposition from 60 vol% heptane, followed by aging in 60 vol% heptane and subsequent rinsing with 40 and 90 vol% heptane, (b) frequency-dissipation plot for n=3 showing whole experiment. Shifts are measured relative to baseline in 0.1 gL^{-1} asphaltenes in 0 vol% heptane.

Thus far we have focused on QCM-D data from the third overtone (n=3) only, however, data from higher overtones (n=5,7,9,11,13) was also collected. Higher overtones are recorded at higher frequencies, where the quartz crystal sensor has a smaller amplitude of oscillation. Penetration depth (δ), the distance from the sensor surface at which the amplitude (A) of the shear wave has decayed to A/e, is calculated by:

$$\delta = \sqrt{\frac{\eta_L}{\pi f \rho_L}} \qquad \text{Equation 5}$$

where η_L is the liquid shear viscosity, ρ_L is the liquid density and f is the frequency of oscillation [41]. This means that higher overtones give information on the nearer-surface region. The penetration depths in toluene and heptane are given in Table 2. Dissipative (e.g. thick, viscous) films adsorbed at the sensor surface can further dampen sensor oscillation and decrease the penetration depth.

Table 2. Penetration depth of quartz crystal shear wave into liquid toluene and heptane at 20°C

Overtone number	f (Hz)	Penetration depth in toluene (nm)	Penetration depth in heptane (nm)
1	5.0E+06	205	164
3	1.5E+07	118	94
5	2.5E+07	92	73
7	3.5E+07	78	62
9	4.5E+07	68	55
11	5.5E+07	62	49
13	6.5E+07	57	45

Frequency-dissipation plots for the experiment shown in Fig 8 are given for all overtones in Fig 9. Note that n=13 was dampened substantially such that it could no longer be monitored by the QCM. Noise in the measurements for n=11 and n=9, particularly at the point where the film is at its thickest / softest is also due to excessive dampening.

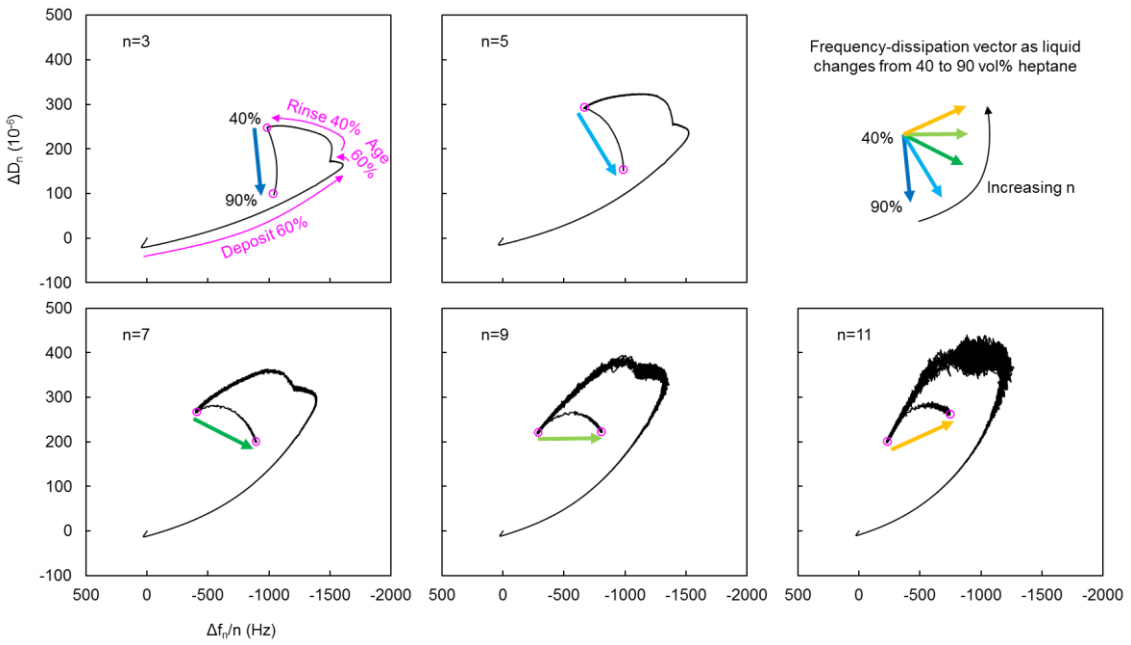

Fig 9. Frequency-dissipation plots for 0.1 gL^{-1} asphaltenes deposition from 60 vol% heptane, followed by aging in 60 vol% heptane and subsequent rinsing with 40 and 90 vol% heptane. The frequency-dissipation vector (arrows) during film contraction as the liquid changes from 40 to 90 vol% heptane depends on overtone number (n). The same scale is used for all plots.

When the quality of the solvent is decreased from 40 to 90 vol% heptane, the swollen film becomes more compact. For lower overtones (n=3) the dissipation decreases significantly, while the frequency remains approximately unchanged, as expected during film contraction without mass-change. However, unexpected behaviour is seen with increasing overtone number. The higher overtones exhibit a very small decrease in dissipation (n=9) or even an increase in dissipation (n=11), but a large decrease in frequency, suggesting that the mass increases (opposite to expected). As the shear wave from the higher overtones cannot penetrate the entire thickness of the deposited film, particularly in the swollen state, the apparent mass sensed by higher overtones increases as the film contracts.

Incongruous behaviour of the higher overtones is also seen at other stages of the experiment. For example, during mass deposition the film appears more dissipative at higher overtones, i.e. steeper gradient of $\Delta D_n/(-\Delta f_n/n)$. Overtone-dependent frequency and dissipation response is an artefact of viscoelastic films [30,42] and depends on the elastic loss modulus on the film [43,44]. The mechanical properties (viscosity and shear modulus) of viscoelastic films which result in maximum dissipation vary depending on overtone number [45]. See, that in our experiment, the point at which dissipation is maximum changes with overtone number (Fig 9).

Another interesting observation is that after aging for approximately 1 h, the fractional mass loss in 40 vol% heptane is lower for a deposit formed at 60 vol% heptane (15% of mass removed) than for one formed at higher 70 vol% heptane (53% of mass removed), Fig 10. This agrees with the earlier observation that deposits formed at lower heptane vol% are less soluble and more difficult to remove (Table 1).

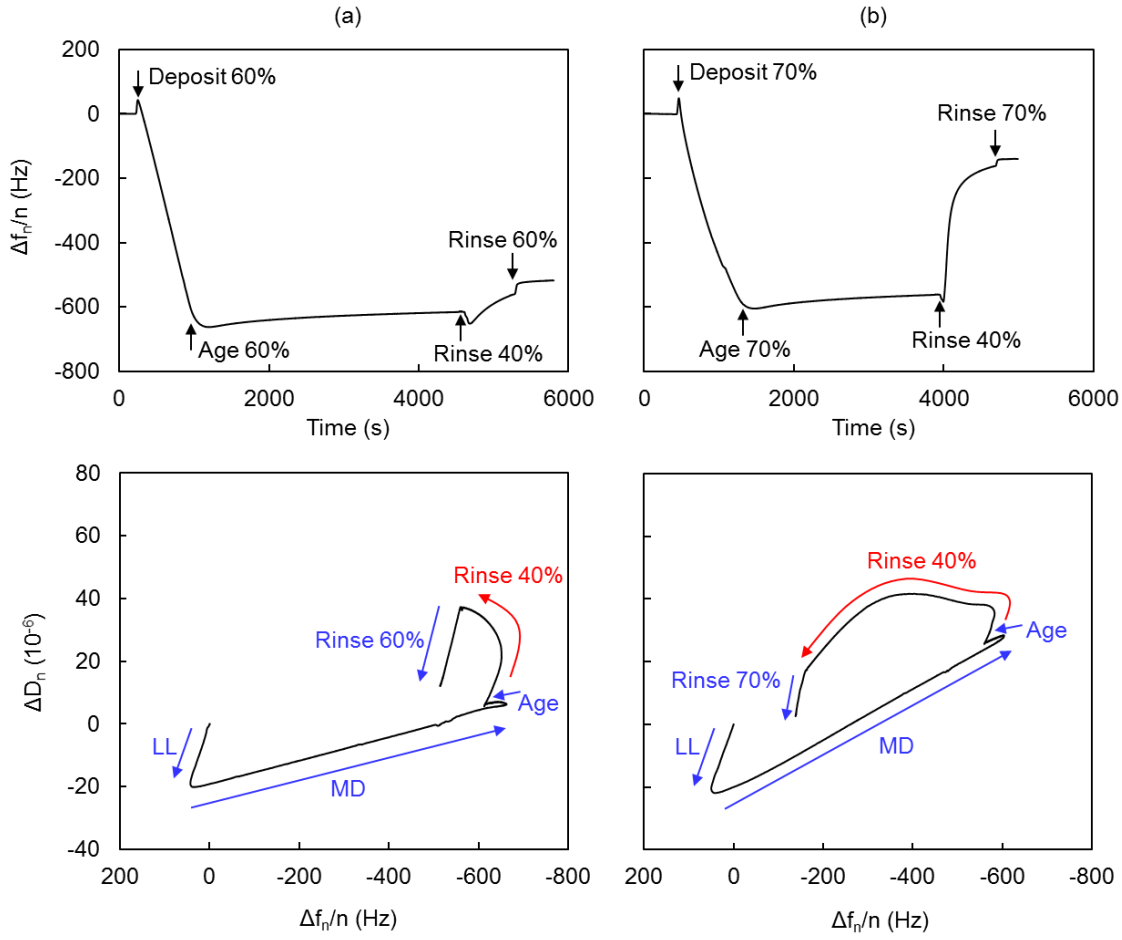

Fig 10. Impact of deposition conditions on deposit removal following aging for approximately 1 h. Frequency vs. time (top) and frequency-dissipation plots for n=3 (bottom) showing 0.1 gL^{-1} asphaltenes deposition from (a) 60 and (b) 70 vol% heptane. Shifts are relative to a baseline in 0.1 gL^{-1} asphaltenes in 0 vol% heptane.

Liquid-cell AFM of asphaltene deposits in different solvent environments

Asphaltene deposition-aging-rinsing experiments were carried out on a steel substrate inside an atomic force microscope (AFM) with a liquid flow cell. Prior to asphaltene deposition, the steel substrate was

scanned in toluene, Fig 11 (a). Polishing scratches are visible on the steel surface. The AFM tip was retracted from the surface and asphaltenes deposited from 70 vol% heptane for a deposition time of 15 min. After deposition, the film was aged in 70 vol% heptane for 1 h before re-engaging the AFM and scanning the deposited film, Fig 11 (b). The deposit appears to have a particulate morphology. Particle size analysis using NanoScope Analysis software shows that the morphology of the uppermost surface of the deposit consists of globular features with mean diameter of 285 nm and height of 23 nm. An area of the thick deposited film was removed by loaded-scanning in contact-mode (scraping with the AFM tip), Fig 11 (d). After removal of the thick deposited film, the polishing marks on the steel substrate are once again visible, Fig 11 (e). Note, it is possible that a thin layer of asphaltenes remains on the surface after loaded-scanning. Using the exposed steel substrate as a reference, it is determined that the thickness of the aged deposited asphaltene film is c. 100 nm, Fig 12 (a). The phase shift for the scraped area generally appears more negative than for the thick deposit, Fig 11 (c). We used a light tapping force (amplitude set point / free amplitude = 0.91), thus changes in phase contrast may depend on changes in roughness and/or topography [46] (see that the edges of particles appear darker) rather than sample stiffness [47,48].

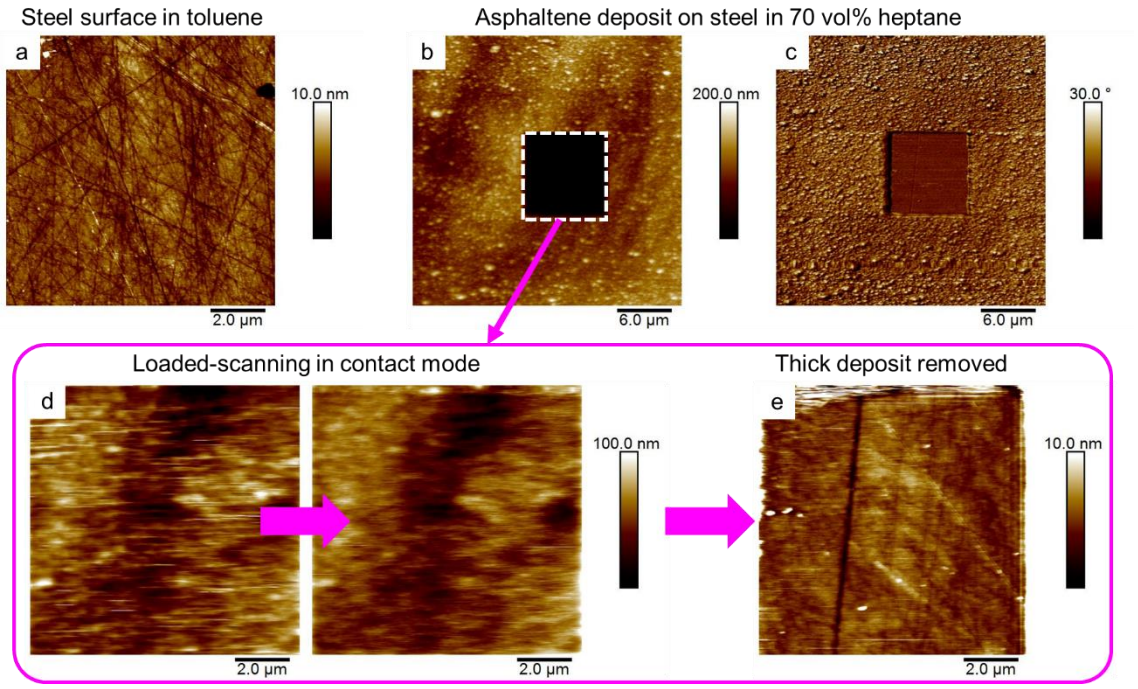

Fig 11. AFM of asphaltene deposit formed in situ inside liquid-cell. Tapping mode height images of (a) steel surface in toluene and (b) aged asphaltene deposit on steel in 70 vol% heptane (outside the black square). (c) Phase image obtained simultaneously with (b). (d) Contact mode AFM height images showing removal of deposit under loaded-scanning at 50 nN and (e) after deposit removal, note difference in z-scale once film removed.

The asphaltene deposit was subsequently rinsed with 40 and 0 vol% heptane. The changing morphology of the deposit is shown in Fig 12. At the point of rinsing with 40 vol% heptane, the total aging time in 70 vol% heptane was 2.5 h. In 40 vol% heptane the deposit is thinner, suggesting some mass-loss. Additionally, particles are no longer visible and the film seems more continuous and smoother, Fig 12 (b). AFM suggests a change in deposit morphology as it swells in 40 vol% heptane. In 0 vol% heptane, most of the deposited asphaltene film is removed and the polishing scratches on the steel substrate are visible. In some regions asphaltene deposits remain, notably accumulated at the sides of the scraped area, indicated by blue arrows in Fig 12 (c).

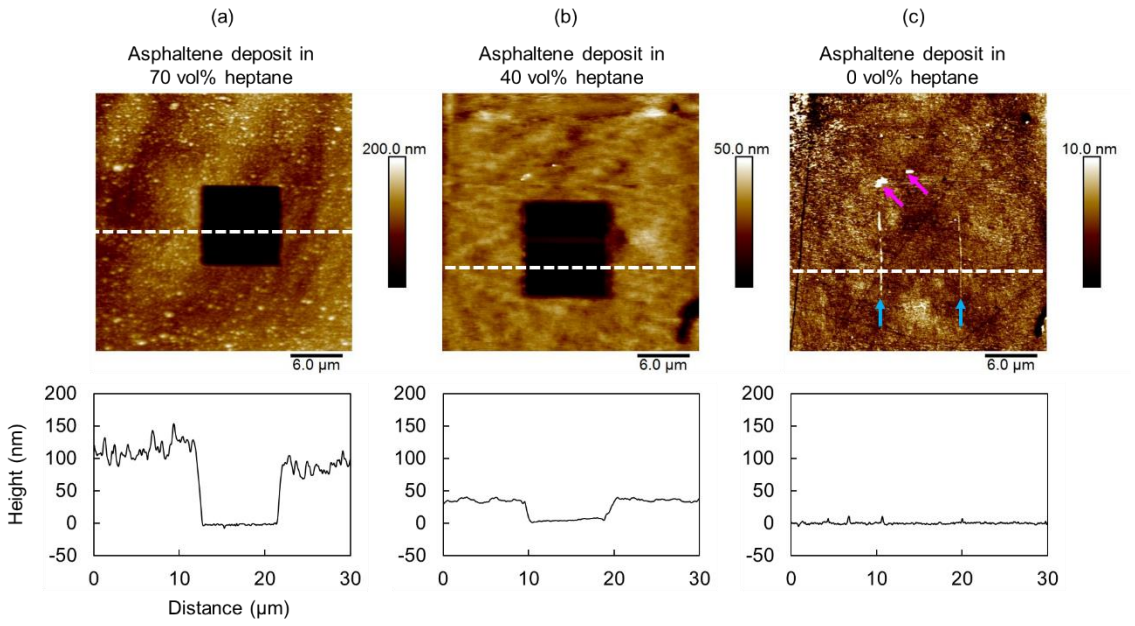

Fig 12. AFM of the same asphaltene deposit in changing heptane-toluene solvent environments from left to right. Tapping mode AFM height images (top) and line profiles (bottom) showing asphaltene deposit in (a) 70, (b) 40 and (c) 0 vol% heptane. In image (c) blue arrows show deposit accumulated at edge of scraped area and pink arrows indicate regions where deposit remains.

Force-separation curves were obtained for the steel substrate in toluene and for the asphaltene deposit in 70, 40 and 0 vol% heptane, Fig 13. Note that separation = 0 nm is a “hard-wall”, i.e. the point at which the applied force increases towards infinity, and is governed by the relative stiffness of the cantilever vs. the sample - it is not an absolute measure of the tip-steel substrate separation. In all cases, a repulsive force is observed as the tip approaches and retracts from the surface. This repulsive force is experienced over a longer distance for the asphaltene deposit than for the bare steel surface, suggesting a thicker soft ad-layer is formed by asphaltenes. A very long-range repulsive force is observed for the deposited film in 40 vol% heptane, suggesting that the film is more swollen in 40% heptane than in 70 vol% heptane. This supports QCM-D observations that asphaltene deposits which have been aged in poor (high-heptane)

solvent swell when the solvent quality is improved. Previously, similar long-range repulsive forces were observed for swollen polymer brushes in different solvent environments [49]. Note that the obtained force curves may describe asphaltene-asphaltene interaction (rather than asphaltene-silicon nitride interaction), since asphaltene deposition on and/or transfer to the AFM tip is possible.

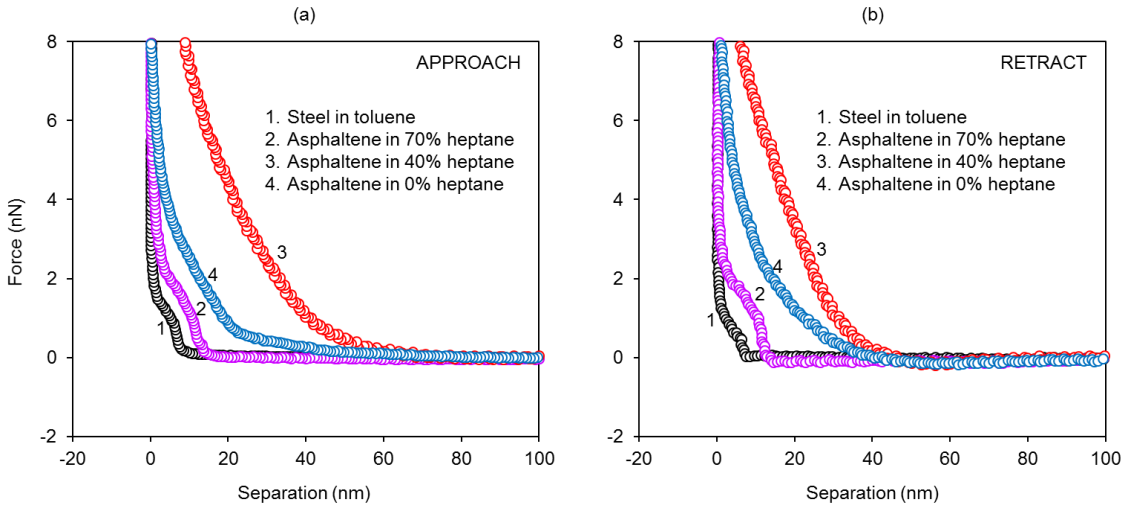

Fig 13. Force curves during (a) approach and (b) retract of AFM tip for steel surface in toluene and asphaltene deposit in different heptane-toluene solvent environments.

Implications for the removal of asphaltene deposits in petroleum production

One of the main findings of this study is that deposits formed under different conditions (heptane-toluene ratios), but from the same asphaltene sample, display different solubilities. This suggests that deposits formed at different positions in the petroleum production pipeline, or even the same position under a different environmental condition, will have different behaviours with regard to their ease of removal. Deposit thickness alone is not a good indicator of how 'easy' it will be to remove a film. The composition of the film and its solvent-environmental history must be considered.

It seems intuitive that the conditions used to destabilize asphaltenes will impact the chemical composition of deposited films. A very strongly destabilizing environment will lead to the deposition of a wider range of asphaltene chemistries, some of which will actually help with subsequent deposit removal in aromatic solvent. Interestingly, these useful chemistries may be removed during rinsing with heptane-toluene. The question remains, what in fact are the chemistries within asphaltenes that facilitate easy deposit removal and dissolution. Previously, high resolution mass spectrometry was used to investigate sub-

fractions of asphaltenes formed by selective adsorption (or not) onto silica [50]. In future, mass spectrometry of deposits formed under different conditions and after different aging times in heptane-toluene could reveal compositional differences. However, pin-pointing the precise chemistries involved may prove challenging given the chemically diverse nature of asphaltenes. An alternative approach would be to investigate whether various synthesized model asphaltene molecules of known chemistry can alter the ease of deposit removal [51,52].

Several limitations of the current study should also be noted. Firstly, an extracted asphaltene sample was used, thus additional chemistries that are present within crude oil will be missing. Resins, for example may co-aggregate and co-deposit with asphaltenes thus impacting deposit removal [53,54,55]. Secondly, we use a gold surface for QCM experiments, in reality oil pipes are made of steel. Although we investigate multilayer deposition onto a pre-formed asphaltene monolayer, which is found to remain intact upon toluene-rinsing, an effect of the underlying substrate cannot be ruled out. Thirdly, the current study focuses on the early stages of multilayer deposition. The later stages of deposit build-up may not be monitored by QCM-D owing to excessive dampening of the quartz sensor. Finally, the morphology of deposited films must be considered. Looser, more open structures may allow easier solvent transport through the deposit and facilitate dissolution.

Conclusions

QCM-D and liquid-cell AFM have been used to investigate the deposition, aging and removal of asphaltene films. In-line mixing of asphaltene solution in toluene with heptane-toluene generated destabilized dispersions of colloidal particles which resulted in surface deposition. Frequency-dissipation plots aided interpretation of QCM-D data because regions of liquid-loading (due to changing heptane-toluene ratio), surface deposition of asphaltenes, deposit aging and film removal by solvent-rinsing could be easily distinguished. This was particularly useful when the properties of the deposited film and the bulk liquid changed simultaneously, since it allowed us to differentiate between the two effects and extract previously hidden information on the properties of asphaltene films during their removal.

Immediate rinsing of deposited films with asphaltene solution in toluene resulted in instantaneous removal of deposits. The properties of unaged deposits did not change appreciably during their removal. Aging of deposited films in poor (high heptane) solvent made subsequent removal of deposits with toluene more difficult. Removal of films was no longer instantaneous, and in some cases a strongly-bound deposit remained on the surface after toluene-rinsing for over 1 h.

The properties of aged deposits were dramatically altered during their removal. Solvent-rinsing of aged deposits with solvents of better quality than the solvent during deposition, i.e. pure toluene or solvent of

lower heptane vol%, lead to swelling of deposited films. Swelling resulted in increased dissipation in QCM-D experiments. Long-range repulsion was also observed during tip-surface approach and retract in AFM measurements. Swelling caused a change in film morphology; the particulate nature of the deposited film was lost and it appeared smoother and more continuous. Swollen films could be contracted (made more rigid) by flowing poor (high heptane) solvent, suggesting that swelling is partly reversible and depends on the quality of the solvent in contact with the film.

Deposits formed at higher heptane vol% are more soluble and easier to remove than those formed at lower heptane vol%. Additionally, dissolved asphaltenes in toluene helped remove deposited films. Hence co-deposited and dissolved more soluble (potentially resinous) asphaltenes may be useful in remediation.

Acknowledgments

We acknowledge the funding and technical support from BP through the BP International Centre for Advanced Materials (BP-ICAM) which made this research possible.

Supporting Information

Supporting information can be found in one document which contains:

1 Viscosity and density of test liquids

2 QCM-D heptane-toluene liquid exchange dynamics

3 QCM-D experiments showing asphaltenes deposition-aging-rinsing under different conditions

4 Determination of deposit removal times from QCM-D data

References

1. Adams, J. J. Asphaltene Adsorption, a Literature Review. *Energy & Fuels* **2014**, *28* (5), 2831–2856 DOI: 10.1021/ef500282p.
2. Yudin, I. K.; Nikolaenko, G. L.; Gorodetskii, E. E.; Kosov, V. I.; Melikyan, V. R.; Markhashov, E. L.; Frot, D.; Briolant, Y. Mechanisms of asphaltene aggregation in toluene–heptane mixtures. *J. Pet. Sci. Eng.* **1998**, *20* (3–4), 297–301 DOI: 10.1016/S0920-4105(98)00033-3.
3. Hoepfner, M. P.; Vilas Bôas Fávero, C.; Haji-Akbari, N.; Fogler, H. S. The Fractal Aggregation of Asphaltenes. *Langmuir* **2013**, *29* (28), 8799–8808 DOI: 10.1021/la401406k.
4. Vilas Bôas Fávero, C.; Maqbool, T.; Hoepfner, M.; Haji-Akbari, N.; Fogler, H. S. Revisiting the flocculation kinetics of destabilized asphaltenes. *Adv. Colloid Interface Sci.* **2017**, *244*, 267–280 DOI: https://doi.org/10.1016/j.cis.2016.06.013.
5. Buckley, J. S. Asphaltene Deposition. *Energy & Fuels* **2012**, *26* (7), 4086–4090 DOI: 10.1021/ef300268s.
6. Seifried, C. M.; Al Lawati, S.; Crawshaw, J. P.; Boek, E. S. Asphaltene Deposition in Capillary Flow. *SPE Annual Technical Conference and Exhibition*. Society of Petroleum Engineers: New Orleans, Louisiana, USA 2013, p 10.
7. Vilas Bôas Fávero, C.; Hanpan, A.; Phichphimok, P.; Binabdullah, K.; Fogler, H. S. Mechanistic Investigation of Asphaltene Deposition. *Energy & Fuels* **2016**, *30* (11), 8915–8921 DOI: 10.1021/acs.energyfuels.6b01289.
8. Chaisoontornyotin, W.; Haji-Akbari, N.; Fogler, H. S.; Hoepfner, M. P. Combined Asphaltene Aggregation and Deposition Investigation. *Energy & Fuels* **2016**, *30* (3), 1979–1986 DOI: 10.1021/acs.energyfuels.5b02427.
9. Hu, C.; Morris, J. E.; Hartman, R. L. Microfluidic investigation of the deposition of asphaltenes in porous media. *Lab Chip* **2014**, *14* (12), 2014–2022 DOI: 10.1039/c4lc00192c.
10. Lin, Y.-J.; He, P.; Tavakkoli, M.; Mathew, N. T.; Fatt, Y. Y.; Chai, J. C.; Goharzadeh, A.; Vargas, F. M.; Biswal, S. L. Examining Asphaltene Solubility on Deposition in Model Porous Media. *Langmuir* **2016**, *32* (34), 8729–8734 DOI: 10.1021/acs.langmuir.6b02376.
11. Lin, Y.-J.; He, P.; Tavakkoli, M.; Mathew, N. T.; Fatt, Y. Y.; Chai, J. C.; Goharzadeh, A.; Vargas, F. M.; Biswal, S. L. Characterizing Asphaltene Deposition in the Presence of Chemical Dispersants in Porous Media Micromodels. *Energy & Fuels* **2017**, *31* (11), 11660–11668 DOI: 10.1021/acs.energyfuels.7b01827.
12. Schuler, B.; Meyer, G.; Peña, D.; Mullins, O. C.; Gross, L. Unraveling the Molecular Structures of Asphaltenes by Atomic Force Microscopy. *J. Am. Chem. Soc.* **2015**, *137* (31), 9870–9876 DOI: 10.1021/jacs.5b04056.
13. Mullins, O. C. The Modified Yen Model. *Energy & Fuels* **2010**, *24* (4), 2179–2207 DOI: 10.1021/ef900975e.
14. Fenistein, D.; Barré, L.; Broseta, D.; Espinat, D.; Livet, A.; Roux, J.-N.; Scarsella, M. Viscosimetric and Neutron Scattering Study of Asphaltene Aggregates in Mixed Toluene/Heptane Solvents. *Langmuir* **1998**, *14* (5), 1013–1020 DOI: 10.1021/la9709148.
15. Hoepfner, M. P.; Limsakoune, V.; Chuenmeechao, V.; Maqbool, T.; Scott Fogler, H. A fundamental study of asphaltene deposition. *Energy and Fuels* **2013**, *27* (2), 725–735 DOI: 10.1021/ef3017392.
16. Maqbool, T.; Balgoa, A. T.; Fogler, H. S. Revisiting Asphaltene Precipitation from Crude Oils: A Case of Neglected Kinetic Effects. *Energy & Fuels* **2009**, *23* (7), 3681–3686 DOI: 10.1021/ef9002236.

17. Spiecker, P. M.; Gawrys, K. L.; Kilpatrick, P. K. Aggregation and solubility behavior of asphaltenes and their subfractions. *J. Colloid Interface Sci.* **2003**, *267* (1), 178–193 DOI: https://doi.org/10.1016/S0021-9797(03)00641-6.

18. Campen, S.; Smith, B.; Wong, J. Deposition of Asphaltene from Destabilized Dispersions in Heptane–Toluene. *Energy & Fuels* **2018** DOI: 10.1021/acs.energyfuels.8b01887.

19. Gabrienko, A. A.; Morozov, E. V; Subramani, V.; Martyanov, O. N.; Kazarian, S. G. Chemical Visualization of Asphaltenes Aggregation Processes Studied in Situ with ATR-FTIR Spectroscopic Imaging and NMR Imaging. *J. Phys. Chem. C* **2015**, *119* (5), 2646–2660 DOI: 10.1021/jp511891f.

20. Carbognani, L. Dissolution of Solid Deposits and Asphaltenes Isolated from Crude Oil Production Facilities. *Energy & Fuels* **2001**, *15* (5), 1013–1020 DOI: 10.1021/ef0100146.

21. Ekholm, P.; Blomberg, E.; Claesson, P.; Auflem, I. H.; Sjöblom, J.; Kornfeldt, A. A quartz crystal microbalance study of the adsorption of asphaltenes and resins onto a hydrophilic surface. *J. Colloid Interface Sci.* **2002**, *247* (2), 342–350 DOI: 10.1006/jcis.2002.8122.

22. Rudrake, A.; Karan, K.; Horton, J. H. A combined QCM and XPS investigation of asphaltene adsorption on metal surfaces. *J. Colloid Interface Sci.* **2009**, *332* (1), 22–31 DOI: 10.1016/j.jcis.2008.12.052.

23. Campen, S.; Di Mare, L.; Smith, B.; Wong, J. S. S. Determining the Kinetics of Asphaltene Adsorption from Toluene: A New Reaction-Diffusion Model. *Energy and Fuels* **2017**, *31* (9) DOI: 10.1021/acs.energyfuels.7b01374.

24. Tavakkoli, M.; Panuganti, S. R.; Vargas, F. M.; Taghikhani, V.; Pishvaie, M. R.; Chapman, W. G. Asphaltene Deposition in Different Depositing Environments: Part 1. Model Oil. *Energy & Fuels* **2014**, *28* (3), 1617–1628 DOI: 10.1021/ef401857t.

25. Richter, R.; Mukhopadhyay, A.; Brisson, A. Pathways of lipid vesicle deposition on solid surfaces: a combined QCM-D and AFM study. *Biophys. J.* **2003**, *85* (5), 3035–3047 DOI: 10.1016/S0006-3495(03)74722-5.

26. Lee, H.-S.; Yee, M. Q.; Eckmann, Y. Y.; Hickok, N. J.; Eckmann, D. M.; Composto, R. J. Reversible swelling of chitosan and quaternary ammonium modified chitosan brush layers: effects of pH and counter anion size and functionality. *J. Mater. Chem.* **2012**, *22* (37), 19605–19616 DOI: 10.1039/C2JM34316A.

27. Liu, G.; Zhang, G. Collapse and Swelling of Thermally Sensitive Poly(N-isopropylacrylamide) Brushes Monitored with a Quartz Crystal Microbalance. *J. Phys. Chem. B* **2005**, *109* (2), 743–747 DOI: 10.1021/jp046903m.

28. Kasemo, B.; Fant, C.; Sott, K.; Elwing, H.; Qcm-d, T. Variations in Coupled Water, Viscoelastic Properties, and Film Thickness of a Mefp-1 Protein Film during Adsorption and Cross-Linking: A Quartz Crystal Microbalance with Dissipation Monitoring, Ellipsometry, and Surface Plasmon. *Anal. Chem.* **2001**, *73* (24), 5796–5804.

29. Liu, L.-S.; Kim, J.; Chang, S.-M.; Choi, G. J.; Kim, W.-S. Quartz Crystal Microbalance Technique for Analysis of Cooling Crystallization. *Anal. Chem.* **2013**, *85* (9), 4790–4796 DOI: 10.1021/ac400585c.

30. Voinova, M. V; Jonson, M.; Kasemo, B. “Missing mass” effect in biosensor’s QCM applications. *Biosens. Bioelectron.* **2002**, *17* (10), 835–841 DOI: https://doi.org/10.1016/S0956-5663(02)00050-7.

31. Reviakine, I.; Johannsmann, D.; Richter, R. P. Hearing what you cannot see and visualizing what you hear: Interpreting quartz crystal microbalance data from solvated interfaces. *Anal. Chem.* **2011**, *83* (23), 8838–8848 DOI: 10.1021/ac201778h.

32. Barrera, D. M.; Ortiz, D. P.; Yarranton, H. W. Molecular weight and density distributions of asphaltenes from crude oils. *Energy and Fuels* **2013**, *27* (5), 2474–2487 DOI: 10.1021/ef400142v.

33. Rogel, E.; Carbognani, L. Density estimation of asphaltenes using molecular dynamics simulations. *Energy & fuels* **2003**, *17* (11), 378–386 DOI: 10.1021/ef020200r.

34. Kanazawa, K. K.; Gordon, J. G. The oscillation frequency of a quartz resonator in contact with liquid. *Anal. Chim. Acta* **1985**, *175* (C), 99–105.

35. Kanazawa, K. K.; Gordon, J. G. Frequency of a quartz microbalance in contact with liquid. *Anal. Chem.* **1985**, *57* (8), 1770–1771.

36. Höök, F.; Rodahl, M.; Brzezinski, P.; Kasemo, B. Energy Dissipation Kinetics for Protein and Antibody−Antigen Adsorption under Shear Oscillation on a Quartz Crystal Microbalance. *Langmuir* **1998**, *14* (4), 729–734 DOI: 10.1021/la970815u.

37. Limson, J.; Odunuga, O. O.; Green, H.; Hook, F.; Blatch, G. L. The use of a quartz crystal microbalance with dissipation for the measurement of protein-protein interactions : a qualitative and quantitative analysis of the interactions between molecular chaperones. *S. Afr. J. Sci.* **2004**, *100* (11–12), 678–682.

38. Fredriksson, C.; Kihlman, S.; Rodahl, M.; Kasemo, B. The Piezoelectric Quartz Crystal Mass and Dissipation Sensor: A Means of Studying Cell Adhesion. *Langmuir* **1998**, *14* (2), 248–251 DOI: 10.1021/la971005l.

39. Vargas, F. M.; Lin, Y.-J. and Biswal, S. L. Advanced strategies for mitigation of asphaltene deposition. 2nd Annual Production Chemical Optimization Unconventional Oil and Gas, Houston, Texas, 29-30 June 2016. https://www.lbcg.com/media/downloads/events/573/pco16-francisco-vargas.10479.pdf

40. Alboudwarej, H.; Beck, J.; Svrcek, W. Y.; Yarranton, H. W.; Akbarzadeh, K. Sensitivity of asphaltene properties to separation techniques. *Energy and Fuels* **2002**, *16* (2), 462–469 DOI: 10.1021/ef010213p.

41. Mecea, V. M. Loaded vibrating quartz sensors. *Sensors Actuators A Phys.* **1994**, *40* (1), 1–27 DOI: https://doi.org/10.1016/0924-4247(94)85026-7.

42. Dunér, G.; Thormann, E.; Dedinaite, A. Quartz Crystal Microbalance with Dissipation (QCM-D) studies of the viscoelastic response from a continuously growing grafted polyelectrolyte layer. *J. Colloid Interface Sci.* **2013**, *408* (1), 229–234 DOI: 10.1016/j.jcis.2013.07.008.

43. Kanazawa, K.; Frank, C. W.; Hardesty, J. Resonances of soft films under liquid on the QCM. *ECS Trans.* **2008**, 16 (11), 419–429 DOI: 10.1149/1.2981147.

44. Kanazawa, K.; Cho, N.-J. Quartz crystal microbalance as a sensor to characterize macromolecular assembly dynamics. *J. Sensors* **2009**, 824947 DOI: 10.1155/2009/824947.

45. McNamara, T. P.; Blanford, C. F. A sensitivity metric and software to guide the analysis of soft films measured by a quartz crystal microbalance. *Analyst* **2016**, *141* (10), 2911–2919 DOI: 10.1039/C6AN00143B.

46. Ye, Z.; Zhao, X. Phase imaging atomic force microscopy in the characterization of biomaterials. *J. Microsc.* **2010**, *238* (1), 27–35 DOI: 10.1111/j.1365-2818.2009.03282.x.

47. Magonov, S. N.; Elings, V.; Whangbo, M.-H. Phase imaging and stiffness in tapping-mode atomic force microscopy. *Surf. Sci.* **1997**, *375* (2), L385–L391 DOI: https://doi.org/10.1016/S0039-6028(96)01591-9.

48. Nagao, E.; Dvorak, J. A. Phase Imaging by Atomic Force Microscopy: Analysis of Living Homoiothermic Vertebrate Cells. *Biophys. J.* **1999**, *76* (6), 3289–3297 DOI: https://doi.org/10.1016/S0006-3495(99)77481-3.

49. Yu, Y.; Kieviet, B. D.; Kutnyanszky, E.; Vancso, G. J.; de Beer, S. Cosolvency-Induced Switching of the Adhesion between Poly(methyl methacrylate) Brushes. *ACS Macro Lett.* **2015**, *4* (1), 75–79 DOI: 10.1021/mz500775w.

50. Nascimento, P. T. H.; Santos, A. F.; Yamamoto, C. I.; Tose, L. V; Barros, E. V; Gonçalves, G. R.; Freitas, J. C. C.; Vaz, B. G.; Romão, W.; Scheer, A. P. Fractionation of Asphaltene by Adsorption onto Silica and Chemical Characterization by Atmospheric Pressure Photoionization Fourier Transform Ion Cyclotron Resonance Mass Spectrometry, Fourier Transform Infrared Spectroscopy Coupled to Attenuated Total Reflectance, and Proton Nuclear Magnetic Resonance. *Energy & Fuels* **2016**, *30* (7), 5439–5448 DOI: 10.1021/acs.energyfuels.6b00523.

51. Gray, M. R.; Tykwinski, R. R.; Stryker, J. M.; Tan, X. Supramolecular Assembly Model for Aggregation of Petroleum Asphaltenes. *Energy & Fuels* **2011**, *25* (7), 3125–3134 DOI: 10.1021/ef200654p.

52. Sjöblom, J.; Simon, S.; Xu, Z. Model molecules mimicking asphaltenes. *Adv. Colloid Interface Sci.* **2015**, *218*, 1–16 DOI: https://doi.org/10.1016/j.cis.2015.01.002.

53. Rogel, E. Molecular Thermodynamic Approach to the Formation of Mixed Asphaltene−Resin Aggregates. *Energy & Fuels* **2008**, *22* (6), 3922–3929 DOI: 10.1021/ef800258p.

54. Sedghi, M.; Goual, L. Role of Resins on Asphaltene Stability. *Energy & Fuels* **2010**, *24* (4), 2275–2280 DOI: 10.1021/ef9009235.

55. Ekholm, P.; Blomberg, E.; Claesson, P.; Auflem, I. H.; Sjöblom, J.; Kornfeldt, A. A Quartz Crystal Microbalance Study of the Adsorption of Asphaltenes and Resins onto a Hydrophilic Surface. *J. Colloid Interface Sci.* **2002**, *247* (2), 342–350 DOI: https://doi.org/10.1006/jcis.2002.8122.

Table of contents graphic